Research Square

Preprints are preliminary reports that have not undergone peer review.
They should not be considered conclusive, used to inform clinical practice,
or referenced by the media as validated information.

Bone Density Architecture and Functional Cortical Thickness of the Greater Tuberosity: A CT-Based Analysis of 739 Proximal Humeri

Milad Farkhondeh Fal
Schoen Clinic Hamburg Eilbek
Franziska Schreiber
University Medical Center Hamburg-Eppendorf
Sarah I. Schmitz
University Medical Center Hamburg-Eppendorf
Luis Enrique Jimenez Garcia
Stryker Trauma GmbH
Bernhard Hofstätter
Stryker Trauma GmbH
Holger Kleinertz
University Medical Center Hamburg-Eppendorf
Darius Thiesen
University Medical Center Hamburg-Eppendorf
Karl-Heinz Frosch
University Medical Center Hamburg-Eppendorf
Lukas F. Heilmann
l.heilmann@uke.de

University Medical Center Hamburg-Eppendorf

Research Article

Keywords: Bone quality, Computed tomography, Hounsfield units, Proximal humerus, Rotator cuff, Osteoporosis

Posted Date: November 9th, 2026

DOI: https://doi.org/10.21203/rs.3.rs-11368202/v1

License: This work is licensed under a Creative Commons Attribution 4.0 International License.
Read Full License

Additional Declarations: No competing interests reported.

Abstract

Background

The greater tuberosity (GT) is central to rotator cuff repair and proximal humerus fracture fixation, yet population-level data on its bone density architecture are lacking. This study characterizes the GT density profile, functional cortical thickness (FCT), and regional concordance with the calcar across age and sex subgroups.

Methods

In this retrospective cross-sectional study, computed tomography (CT)-derived Hounsfield unit (HU) values were analyzed in 739 left proximal humeri from a large CT-based bone morphometry database. A 5 mm cylindrical region of interest spanning the GT from posterior to anterior cortex (specimen-specific length, 25.5 ± 3.2 mm) sampled density at 21 points (5% relative-depth increments). Functional cortical thickness (FCT-200) was the number of consecutive increments from the posterior surface at or above 200 HU. Analyses comprised linear and logistic regression, ANCOVA and paired t-tests.

Results

The GT exhibited a U-shaped density profile: 320.9 HU at the posterior surface, a minimum of 7.1 HU at 45% relative depth, and 200.3 HU at the anterior cortex. Age explained 23.1% of variance (− 12.7 HU per decade; $p < 0.001$); sex explained an additional 4.9%. The cortical shell showed the largest absolute decline (− 22.7 HU per decade). In women older than 65 years, FCT-200 did not exceed one increment (≈ 1.15 mm) in 69.2%; in women, the probability of this finding exceeded 50% by age 56 (bootstrap 95% confidence interval [CI]: 50–61). Mean GT density was lower than calcar density in all age and sex subgroups ($\Delta = -48.5$ HU; paired $d = -0.80$; $r = 0.716$), so a 100 HU threshold classified 63.1% of specimens as low density at the GT but 40.7% at the calcar.

Conclusions

The GT has a U-shaped density architecture with a thin functional cortical shell that shows the largest absolute age-related decline; reduced functional cortical thickness in women is already common from the sixth decade. Because the GT is, on average, the lower-density site in all age and sex subgroups, calcar-derived density thresholds should not be assumed to be transferable to the GT. These data provide reference values that may inform anchor fixation and fracture management.

Background

The greater tuberosity (GT) of the proximal humerus serves as the attachment site of the rotator cuff tendons and is central to both degenerative and traumatic shoulder pathology. Surgical repair of rotator cuff tears — one of the most frequently performed shoulder procedures — relies on suture anchor fixation into the GT to reattach torn tendon to bone [1–3]. GT bone quality is equally important in fracture fixation of the proximal humerus, where screw purchase in the tuberosity determines construct stability, and in reverse shoulder arthroplasty with GT osteotomy, where tuberosity reattachment depends on adequate bone stock [4].

Barber et al. reported differences in suture anchor pullout strength within the greater tuberosity [5], and the mechanical properties of trabecular bone directly influence anchor fixation [6]. In osteoporotic bone, anchors may fail to achieve adequate purchase, leading to pullout and repair failure [7–8]. This is particularly relevant for all-suture anchors, which achieve fixation through subcortical deployment within a narrow cortical shell, and for screw-type anchors, which depend on thread purchase along the full insertion depth [9–10]. Furthermore, Tingart et al. were able to show in a cadaveric pQCT study that the pull-out strength of metal screw-type anchors correlated with cortical, but not trabecular, volumetric bone mineral density of the GT [11]. Current anchor selection does not routinely incorporate objective, site-specific bone quality assessment, even though preoperative CT imaging — which could provide such assessment — is available in many clinical workflows and biomechanical studies were able to show that local bone properties significantly influence anchor fixation [6, 12].

Despite the clinical importance of GT bone quality for implant fixation, to date, population-level density data for this region are sparse. Previous studies have characterized the proximal humerus using dual-energy X-ray absorptiometry (DXA), peripheral quantitative computed tomography (pQCT), or micro-CT, but these were limited by small sample sizes (typically $n < 50$), lack of depth-resolved spatial information, or focus on regions other than the GT [13–16]. Using micro-CT, Meyer et al. were able to show that the cancellous bone volume fraction of the GT is only about one quarter to one half of that beneath the articular surface, and that full-thickness rotator cuff tears are associated with a marked further loss of cancellous bone, leaving a largely hollow tuberosity enclosed by a preserved cortical shell [17]. These observations, however, were based on 14 cadaveric humeri from seven elderly donors. No study has reported a depth-resolved density profile of the GT across a large, demographically diverse cohort.

The Stryker Orthopaedic Modeling and Analytics (SOMA) platform provides access to a large CT-based bone morphometry database with three-dimensionally registered anatomical models, enabling standardized density measurements across hundreds of specimens [18–20]. Using this platform, we have previously characterized calcar bone density in the same cohort (companion analysis; submitted for publication).

Therefore, the aim of the present study was to (1) characterize the bone density architecture of the GT in a large population sample, (2) quantify age- and sex-dependent density changes including functional cortical thickness, and (3) assess the regional concordance between GT and calcar density within the

same specimens. Our hypothesis was that the GT would exhibit a characteristic density architecture with substantial age-related decline, that the cortical shell would be the zone most affected by age-related bone loss, and that GT and calcar density would be correlated within specimens.

Methods

Study Design and Data Source

This retrospective cross-sectional imaging study was conducted and reported in accordance with the Strengthening the Reporting of Observational Studies in Epidemiology (STROBE) guidelines (checklist provided as Additional file 1). The study population and imaging methodology have been described in detail in a companion analysis of calcar bone density in the same cohort (submitted for publication); key methodological aspects are described here.

A total of 739 left proximal humeri from skeletally mature individuals (age ≥ 18 years) were included from the SOMA database (Stryker Trauma GmbH, Schönkirchen, Germany). Left humeri were selected to standardize laterality. All eligible specimens in the database were included to maximize statistical power for subgroup analyses; no a priori sample size calculation was performed. Scans were excluded if they showed prior fracture, implant, deformity, tumor, or relevant motion or metal artifact involving the proximal humerus. Specimens with evidence of skeletal immaturity were excluded. Of 742 left humeri meeting the database query criteria, density profiles were available for 739, which formed the study population.

All imaging data were fully anonymized before access and analysis. This study was conducted in accordance with the Declaration of Helsinki. The Ethics Committee of the Hamburg Medical Association (Ethikkommission der Ärztekammer Hamburg; reference number 2023-300394-WF) confirmed that formal ethical approval was not required for this study, as it exclusively used fully anonymized imaging data.

CT Acquisition and Image Processing

Computed tomography (CT) examinations were acquired between 2008 and 2020 at multiple institutions. To reduce inter-scanner variability, each proximal humerus was registered to a standardized three-dimensional coordinate system using the validated SOMA morphometric framework [18–20]. This registration allowed consistent anatomical placement of regions of interest across all specimens regardless of individual bone morphology, limb orientation during imaging, or scanner characteristics.

Bone density was quantified in Hounsfield units (HU). Although HU values do not represent absolute bone mineral density in the absence of phantom calibration, they serve as a widely accepted and clinically practical proxy for local trabecular bone quality, with established correlations to bone mineral density, mechanical strength, and implant fixation [21, 22].

Region of Interest Definition

The primary region of interest (ROI) was a cylindrical volume (5 mm diameter) placed along the anteroposterior axis of the GT footprint, spanning from the posterior to the anterior cortical surface (Fig. 1). The cylinder was defined by two reference landmarks on the posterior and anterior GT cortex, so that its length was specimen-specific and reflected the anteroposterior dimension of the individual GT. This axis was chosen to capture the complete cross-sectional architecture of the GT between two cortical boundaries. Density values were extracted at 5% increments along the cylinder axis (0–100%), generating a density profile with 21 equidistant measurement points. Depth is therefore expressed as relative depth (percentage of cylinder length); the corresponding spatial increment (cylinder length/20) was specimen-specific and is reported in the Results. As a measure of placement consistency, the perpendicular distance from the cylinder center to the superior cortex of the GT was recorded for each specimen.

The cylinder thus samples the full cross-sectional bone architecture of the GT, capturing both cortical surfaces and the intervening cancellous bone. For intra-specimen comparison, a cylindrical ROI of fixed length (30 mm, 5 mm diameter, 21 measurement points at 1.5 mm increments) was placed along the inferomedial calcar, as described previously (companion analysis; submitted for publication). For comparisons between sites, the mean HU across all 21 points was used for each ROI. For visualization, an averaged bone model was generated for each age and sex subgroup, and density heatmaps were obtained on a cutting plane through the humeral head at the level of the GT cylinder (Amira 2020.3; Thermo Fisher Scientific).

Outcome Measures

The primary outcome measures were (1) the mean HU value across all 21 depth points for each specimen, (2) the depth-resolved HU profile from 0% to 100%, and (3) the paired difference between GT and calcar density within each specimen. Secondary outcomes included regression model parameters (age, sex, interaction), threshold analysis (proportion of specimens below 100 HU and 50 HU), depth-zone densities, and functional cortical thickness (FCT). Three depth zones were defined in relative depth: cortical shell (0–10%), subcortical zone (15–30%), and deep cancellous center (35–65%). FCT was defined as the number of consecutive measurement points from the posterior cortical surface (0%) at or above a given HU threshold. Because the sampling increment differed between specimens, FCT is reported primarily in increments; a millimeter equivalent was calculated for each specimen by multiplying the number of increments by that specimen's own increment. The category "FCT ≤ 1 increment" denotes specimens in which only the surface measurement point (or none) reached the threshold, i.e., the functional cortex was thinner than the resolution of the profile. FCT was calculated at 200 HU and 100 HU thresholds. The 200 HU threshold was chosen empirically to approximate the cortical–cancellous transition observed in the depth-resolved density profiles, while the 100 HU threshold is consistent with HU values associated with osteopenic bone mineral density in both the

lumbar spine (mean ~ 101 HU [22]) and the proximal humerus (mean ~ 103 HU [23]). Because the cylinder traverses the GT from posterior to anterior cortex, the FCT at 0% depth reflects the posterior cortical shell thickness. As the sampling increment and the spatial resolution of clinical CT may exceed the true thickness of the GT cortex, FCT is a resolution-limited functional measure of near-surface bone density rather than a measurement of anatomical cortical thickness.

Statistical Analysis

Continuous variables were assessed for normality using the Shapiro–Wilk test and visual inspection. Descriptive statistics are reported as mean ± standard deviation (SD). Comparisons between GT and calcar density used paired t-tests with the paired Cohen's d (mean difference divided by the SD of the differences) as the effect size. Sex differences within age groups were analyzed using independent-samples t-tests with Cohen's d (pooled SD). Differences among age groups were assessed using Bonferroni-corrected pairwise comparisons.

Simple and multiple linear regression models were constructed to evaluate the relationships between age, sex, and GT density. Residual homoscedasticity was assessed using the Breusch-Pagan and White tests. A main-effects model included age and sex (coded as male = 1, female = 0); a full model additionally included the age × sex interaction term. The additional variance explained by sex is reported as the increase in R^2 over the age-only model. A two-way analysis of covariance (ANCOVA) with Type II sums of squares, based on the main-effects model, provided partial η^2 for age and sex. In a sensitivity analysis, ethnicity (Asian vs. all other) was added to the main-effects model. The Pearson correlation coefficient assessed the within-specimen association between GT and calcar density and between FCT-200 and mean GT density.

For subgroup-specific GT–calcar comparisons where the calcar-to-GT variance ratio exceeded 2:1, Glass's δ (using the GT standard deviation as denominator) was reported in addition to the paired d. GT–calcar concordance was assessed by cross-tabulating specimens above and below 100 HU at both sites, yielding conditional probabilities of low GT density given low calcar density and vice versa. Because conditional probabilities obtained with a single absolute threshold depend on the prevalence of low density at each site, the cross-tabulation was repeated with a prevalence-matched GT threshold (the GT percentile corresponding to the proportion of specimens with calcar density < 100 HU). The age dependence of the GT–calcar difference was assessed by linear regression of the within-specimen difference on age. The proportion of specimens in which GT density exceeded calcar density was reported, and a partial correlation between GT and calcar density adjusted for age and sex was calculated.

Posterior-anterior asymmetry of the GT density profile was evaluated by comparing the mean density of the posterior half (0–45% depth) with the anterior half (55–100% depth) using paired t-tests. Because the profile consists of 21 points, the central point (50% depth) was assigned to neither half, so that each half comprised ten measurement points. Depth-specific age effects were assessed by simple linear

regression of HU on age at individual depth points and for each depth zone; relative decline was expressed as the slope per decade divided by the zone mean in young males (18–40 years; n = 121). The proportion of specimens with negative mean HU at mid-GT depth (40–60%) was reported as an indicator of fat- or marrow-dominated bone. Cylinder length was compared between sexes using an independent-samples t-test and correlated with body height (Pearson).

Non-linearity of the age–density relationship was assessed in an exploratory analysis by comparing a quadratic model and a two-segment model against the linear baseline using F-tests. In the two-segment model, separate linear regressions (each with its own intercept) were fitted below and above a candidate breakpoint; candidate breakpoints were tested at 5-year intervals from age 40 to 70, and the breakpoint maximizing R^2 is reported. Because the breakpoint was selected from seven candidates, the corresponding F-test p-values are not adjusted for this selection. As a sensitivity analysis, a continuous segmented model (linear spline without discontinuity at the breakpoint) was fitted. Non-linear models were fitted for the whole cohort and, for the two-segment model, separately for each sex. For the female subgroup, logistic regression was used to estimate the age at which 50% of specimens crossed clinically relevant thresholds (mean GT density < 50 HU; FCT-200 ≤ 1 increment). Bootstrap resampling (2,000 iterations) provided 95% confidence intervals (CIs) for the crossing ages.

Statistical significance was set at $\alpha = 0.05$. All analyses were performed in Python (v3.10) using SciPy (v1.15), statsmodels (v0.14), and pandas. During the preparation of this manuscript, a generative AI tool (Claude, Anthropic, San Francisco, CA) was used to support drafting and editing of the text and the statistical analysis code. The authors reviewed and edited all AI-generated content and take full responsibility for all content of the manuscript. All results are given as mean ± SD unless stated otherwise.

Results

Demographics

A total of 739 proximal humeri were analyzed, comprising 424 male (57.4%) and 315 female (42.6%) specimens. Mean age was 59.2 ± 20.7 years (range 18–101). Specimens were categorized into three age groups: 18–40 years (n = 169; 121 male, 48 female), 41–65 years (n = 243; 135 male, 108 female), and > 65 years (n = 327; 168 male, 159 female). The cohort was predominantly White (80.0%), with 16.9% Asian and 3.1% other or unknown ethnicity (Table 1).

Table 1
Demographic characteristics of the study population and greater tuberosity cylinder length.

n	Overall	Male	Female
	739	**424**	**315**
Age (years), mean ± SD	59.2 ± 20.7	55.8 ± 21.0	63.7 ± 19.3
Age 18–40 years, n (%)	169 (22.9%)	121 (28.5%)	48 (15.2%)
Age 41–65 years, n (%)	243 (32.9%)	135 (31.8%)	108 (34.3%)
Age > 65 years, n (%)	327 (44.2%)	168 (39.6%)	159 (50.5%)
Ethnicity – White, n (%)	591 (80.0%)	342 (80.7%)	249 (79.0%)
Ethnicity – Asian, n (%)	125 (16.9%)	64 (15.1%)	61 (19.4%)
Ethnicity – Other/unknown, n (%)	23 (3.1%)	18 (4.2%)	5 (1.6%)
GT cylinder length (mm), mean ± SD	25.5 ± 3.2	27.4 ± 2.4	23.0 ± 2.3

Cylinder Geometry and Placement

The GT cylinder measured 25.5 ± 3.2 mm (range 9.2–34.1 mm) from posterior to anterior cortex and was longer in male than in female specimens (27.4 ± 2.4 vs. 23.0 ± 2.3 mm; $p < 0.001$). The corresponding sampling increment was 1.28 ± 0.16 mm (range 0.46–1.71 mm; male 1.37 mm, female 1.15 mm). Cylinder length correlated with body height in the subsample with available height data ($r = 0.595$; $n = 347$). The perpendicular distance from the cylinder center to the superior cortex of the GT was 11.3 ± 1.2 mm (range 5.9–16.3 mm).

Greater Tuberosity Density by Age and Sex

Shapiro–Wilk tests indicated statistically significant deviations from normality of the mean HU distribution for the overall cohort ($p < 0.001$) and in four of six subgroups; given the large subgroup sizes, parametric analyses were retained.

Overall mean GT density was 85.2 ± 54.7 HU. Young males (18–40 years) had the highest mean density (133.9 ± 49.1 HU), and older women (> 65 years) the lowest (50.1 ± 40.4 HU). The sex difference was not statistically significant in the youngest group (133.9 vs. 119.4 HU; Cohen's $d = 0.29$; $p = 0.091$), was largest in the 41–65 age group (95.8 vs. 64.4 HU; difference 31.4 HU; $d = 0.71$; $p < 0.001$), and remained similar in the > 65 age group (78.3 vs. 50.1 HU; difference 28.2 HU; $d = 0.60$; $p < 0.001$) (Table 2). All pairwise age-group differences in mean GT density were statistically significant after Bonferroni correction (all $p < 0.001$).

Table 2
Greater tuberosity and calcar mean bone density (HU) by age and sex subgroup.

Subgroup	n	GT (HU)	Calcar (HU)	Δ GT−Calcar (HU)	Paired d	Glass's δ	p
Male 18–40	121	133.9 ± 49.1	222.5 ± 81.5	−88.7 ± 63.7	−1.39	−1.81	< 0.001
Female 18–40	48	119.4 ± 52.2	174.0 ± 65.4	−54.6 ± 52.2	−1.05	—	< 0.001
Male 41–65	135	95.8 ± 46.1	158.0 ± 67.8	−62.1 ± 58.3	−1.07	−1.35	< 0.001
Female 41–65	108	64.4 ± 42.2	102.2 ± 71.7	−37.8 ± 52.3	−0.72	−0.90	< 0.001
Male > 65	168	78.3 ± 51.9	122.9 ± 66.4	−44.6 ± 53.2	−0.84	—	< 0.001
Female > 65	159	50.1 ± 40.4	65.8 ± 64.6	−15.7 ± 55.9	−0.28	−0.39	< 0.001
Overall	739	85.2 ± 54.7	133.6 ± 86.6	−48.5 ± 60.9	−0.80	—	< 0.001

Δ, paired difference GT − calcar. Paired d = mean difference / SD of differences. Glass's δ (GT SD as denominator) is given for age–sex subgroups in which the calcar-to-GT variance ratio exceeded 2:1. p values from paired t-tests.

Depth-Resolved Density Profile

The GT exhibited a characteristic U-shaped density profile along its anteroposterior axis (Fig. 2). Density was highest at the posterior cortical surface (320.9 HU at 0% depth), declined steeply through the subcortical layers (227.6 HU at 5%, 154.4 HU at 10%), reached a minimum of 7.1 HU at 45% relative depth (on average 11.5 mm from the posterior surface), and then recovered toward the anterior cortex (200.3 HU at 100% depth). This U-shape — reflecting the cortex–cancellous–cortex architecture of the GT — was present in all subgroups but flattened progressively with age (Fig. 3): the surface density in older women (253.5 HU) was 39% lower than in young males (414.7 HU), and the trough was deeper (minimum − 16.4 HU at 50% depth in older women vs. 43.0 HU at 45% depth in young males). Mean HU values at all 21 relative depths are given for each subgroup in Additional file 2.

The density profile was asymmetric: the posterior half (0–45% depth) had significantly higher mean density than the anterior half (55–100% depth) across the entire cohort (99.7 vs. 78.2 HU; Δ = 21.5 HU; $p < 0.001$). This asymmetry persisted in all subgroups but narrowed in older men (Δ = 8.8 HU).

Age and Sex as Predictors of GT Density

Simple linear regression showed that age was the dominant predictor of GT density (HU = 160.6 − 1.27 × Age; $R^2 = 0.231$; $p < 0.001$), corresponding to a decline of 12.7 HU per decade (95% CI 11.1–14.4; Fig. 4).

Residual homoscedasticity was confirmed by the Breusch-Pagan test ($p = 0.787$) and White's test ($p = 0.832$). Adding sex increased R^2 to 0.281, i.e., sex explained an additional 4.9% of the variance (ANCOVA partial η^2 for sex = 0.064; for age = 0.205). In the main-effects model, males had 25.0 HU (95% CI 18.1–31.9; $p < 0.001$) higher GT density than females at a given age. The age × sex interaction was not significant ($p = 0.793$) and did not increase R^2, indicating parallel rates of decline in both sexes. In a sensitivity analysis, Asian ethnicity was associated with lower GT density after adjustment for age and sex (− 25.5 HU; 95% CI − 34.4 to − 16.6; $p < 0.001$; adjusted R^2 0.279 → 0.308), whereas the age and sex coefficients were essentially unchanged (− 1.09 vs. −1.16 HU/year; 24.5 vs. 25.0 HU).

The relationship between age and GT density was not strictly linear. A quadratic model ($R^2 = 0.257$; F-test vs. linear: $F = 25.4$, $p < 0.001$) and a two-segment model with a breakpoint at age 60 ($R^2 = 0.258$; $F = 13.0$, $p < 0.001$) both provided modest improvement over the linear fit. In both models, the rate of density decline decelerated with advancing age: the two-segment model estimated a slope of − 1.97 HU/year up to age 60 versus − 0.38 HU/year thereafter. In women, the R^2-maximizing breakpoint was 55 years (− 1.86 vs. −0.24 HU/year; $R^2 = 0.270$; $F = 10.6$), although the fit at 60 years was virtually identical; in men, it was 40 years (− 3.25 vs. −0.70 HU/year; $R^2 = 0.224$; $F = 7.7$), i.e., at the lower boundary of the tested range. A continuous segmented model (no discontinuity at the breakpoint), each at its R^2-maximizing breakpoint, yielded nearly identical fit ($R^2 = 0.258$ overall, 0.270 in women, 0.223 in men).

Depth-Specific Age Effects

Age-related density decline was not uniform across the GT depth profile. The cortical surface (0% depth) exhibited the steepest absolute decline (slope − 2.64 HU/year; $R^2 = 0.198$), and the near-surface point (5% depth) had the highest age-predictive value (slope − 2.31 HU/year; $R^2 = 0.251$). The cortical shell (0–10% depth) declined by 22.7 HU per decade, compared with 12.3 HU per decade in the subcortical zone (15–30%) and 10.5 HU per decade in the deep cancellous center (35–65%). Relative to the respective mean in young males, however, the decline was largest in the deep cancellous center (− 19.0% per decade) and smallest in the cortical shell (− 7.1% per decade). The central trough (45% depth) declined by − 0.95 HU/year ($R^2 = 0.160$). This differential absolute decline produced a progressive flattening of the U-curve: in young males, the surface-to-minimum gradient was 372 HU (414.7 to 43.0 HU), whereas in older women it was 270 HU (253.5 to − 16.4 HU), a 27% compression of the density range.

Functional Cortical Thickness

At the 200 HU threshold, FCT-200 decreased from 2.9 ± 1.2 increments (4.0 ± 1.6 mm) in young males to 1.2 ± 1.0 increments (1.4 ± 1.2 mm) in older women (Table 3). The proportion of specimens with FCT-200 ≤ 1 increment (i.e., at most the surface measurement point at or above 200 HU) increased from 13 out of 121 young males (10.7%) to 66 out of 108 women aged 41–65 years (61.1%) and 110 out of 159 older women (69.2%) (Table 3; Fig. 5); in older women, one increment corresponded to 1.15 ± 0.12 mm, and 38 of these 110 specimens did not reach 200 HU even at the surface point. At the 100 HU threshold, FCT-100 ranged from 6.5 ± 4.8 increments (8.8 ± 6.5 mm) in young males to 2.9 ± 1.9 increments (3.4 ± 2.5 mm) in older women (Table 3). FCT-200 and mean GT density were correlated (Pearson $r = 0.770$; R^2

= 0.593), indicating that functional cortical thickness captures information not fully reflected in mean density alone.

Table 3
Functional cortical thickness (FCT) of the greater tuberosity by age and sex subgroup.

Subgroup	n	FCT-200 (increments)	FCT-200 (mm)	FCT-200 ≤ 1 increment, n (%)	FCT-100 (increments)	FCT-100 (mm)
Male 18–40	121	2.9 ± 1.2	4.0 ± 1.6	13 (10.7%)	6.5 ± 4.8	8.8 ± 6.5
Female 18–40	48	2.6 ± 1.2	2.9 ± 1.4	6 (12.5%)	6.0 ± 4.8	6.6 ± 4.7
Male 41–65	135	2.0 ± 1.2	2.8 ± 1.7	48 (35.6%)	4.1 ± 2.1	5.7 ± 2.9
Female 41–65	108	1.3 ± 0.9	1.5 ± 1.1	66 (61.1%)	3.4 ± 3.2	4.0 ± 4.0
Male > 65	168	1.5 ± 1.9	2.1 ± 2.5	95 (56.5%)	3.7 ± 2.9	5.0 ± 3.9
Female > 65	159	1.2 ± 1.0	1.4 ± 1.2	110 (69.2%)	2.9 ± 1.9	3.4 ± 2.5
Overall	739	1.8 ± 1.4	2.3 ± 2.0	338 (45.7%)	4.2 ± 3.4	5.3 ± 4.5

FCT at the 200 HU and 100 HU thresholds is given in sampling increments (5% of the specimen-specific cylinder length) and as a millimeter equivalent calculated per specimen (increments × individual increment length).

Threshold Analysis

Among female specimens aged 41–65 years, 93 out of 108 (86.1%) had mean GT density below 100 HU. In female specimens older than 65 years, 138 out of 159 (86.8%) were below 100 HU and 96 out of 159 (60.4%) below 50 HU. At mid-GT depth (40–60%), 74.2% of female specimens older than 65 years had negative mean HU values, indicating fat- or marrow-dominated bone.

Age at Threshold Crossing in Women

Logistic regression was used to estimate the age at which 50% of female specimens crossed clinically relevant thresholds. For mean GT density below 50 HU, the 50% crossing age was 69.4 years (bootstrap 95% CI: 63.7–76.2), with the predicted probability rising from 30% at age 50 to 51% at age 70 and 66% at age 85. For FCT-200 ≤ 1 increment, the 50% crossing age was 56.2 years (bootstrap 95% CI: 50.4–61.2), with the probability increasing from 43% at age 50 to 65% at age 70 and 79% at age 85.

Cortical Shell and Cancellous Architecture

The cortical shell of the GT (0–10% relative depth; on average 0–2.6 mm from the posterior surface) had a mean density of 234.3 ± 95.8 HU overall, declining from 317.9 HU in young males to 180.1 HU in older women — below the 200 HU threshold (Table 4). Beyond the cortical shell, density dropped rapidly: the subcortical zone (15–30%; on average 3.8–7.7 mm) averaged 65.0 HU overall but only 36.3 HU in older women, and the deep cancellous center (35–65%; on average 8.9–16.6 mm) averaged 16.2 HU overall and − 10.4 HU in older women, indicating marrow-dominated bone at the GT center in this population.

Table 4
Mean bone density (HU) by depth zone along the anteroposterior axis of the GT.

Subgroup	n	Cortical shell (0–10%)	Subcortical (15–30%)	Deep cancellous (35–65%)
Overall	739	234.3 ± 95.8	65.0 ± 55.9	16.2 ± 49.4
Male 18–40	121	317.9 ± 87.9	114.2 ± 50.8	55.5 ± 45.8
Female 18–40	48	303.1 ± 95.2	97.4 ± 54.3	48.3 ± 48.3
Male 41–65	135	256.9 ± 85.1	73.0 ± 46.9	19.2 ± 40.7
Female 41–65	108	200.4 ± 76.8	42.5 ± 40.6	3.9 ± 41.7
Male > 65	168	209.3 ± 81.9	55.4 ± 53.5	9.5 ± 48.8
Female > 65	159	180.1 ± 73.5	36.3 ± 47.6	−10.4 ± 40.7

Zones are defined in relative depth: cortical shell (0–10%; on average 0–2.6 mm), subcortical zone (15–30%; on average 3.8–7.7 mm), and deep cancellous center (35–65%; on average 8.9–16.6 mm).

GT–Calcar Comparison and Concordance

GT density was significantly lower than calcar density in all subgroups (overall paired difference − 48.5 ± 60.9 HU; paired d = − 0.80; $p < 0.001$; Table 2). The calcar-to-GT variance ratio exceeded 2:1 in four of six subgroups (young males, middle-aged males, middle-aged females, and older females); Glass's δ in these subgroups ranged from − 1.81 in young males to − 0.39 in older females. The GT–calcar difference narrowed with age (+ 9.4 HU per decade; 95% CI 7.4–11.5; $p < 0.001$), because calcar density declined faster than GT density (− 22.2 vs. −12.7 HU per decade). Within individual specimens, GT and calcar density were strongly correlated (Pearson r = 0.716; $p < 0.001$; partial r adjusted for age and sex = 0.587). At the individual level, GT density exceeded calcar density in 19.4% of specimens (range across subgroups 6.6% in young males to 36.5% in older women).

Using a common threshold of 100 HU, 63.1% of specimens were classified as low density at the GT but only 40.7% at the calcar. Consequently, 275 out of 301 specimens (91.4%) with calcar density below 100 HU also had GT density below 100 HU, whereas 275 out of 466 specimens (59.0%) with GT density below 100 HU had calcar density below this threshold. The ratio of the two conditional probabilities

(91.4/59.0 = 1.55) equals the ratio of the prevalences of low density at the two sites (63.1/40.7 = 1.55), so the asymmetry at a common 100 HU threshold is fully explained by the lower overall density of the GT. With a prevalence-matched GT threshold (GT < 65.2 HU, 40.7th percentile), 73.1% of specimens classified as low density at one site were also classified as low density at the other.

Discussion

The most important finding of this study is that the greater tuberosity exhibits a characteristic U-shaped bone density architecture with a thin functional cortical shell that shows the largest absolute age-related decline of any GT zone; in the majority of female specimens older than 65 years, the functional cortex at the 200 HU threshold did not extend beyond a single sampling increment (approximately 1.15 mm in this group). Furthermore, the GT was, on average, the lower-density site compared with the calcar in all age and sex subgroups, so that density thresholds derived from the calcar classify a substantially different proportion of specimens as low density when applied to the GT.

Comparison with Prior Literature

Previous studies have characterized proximal humeral bone density using various imaging modalities but without the spatial resolution or sample size of the present analysis. Tingart et al. characterized the three-dimensional bone density distribution of the proximal humerus using pQCT, finding higher trabecular density in the posterior than in the anterior greater tuberosity [13] and later showed that these regional density differences affect cancellous screw fixation strength [14]. Spross et al. proposed the deltoid tuberosity index as a radiographic proxy for bone quality [15]. More recently, Yu et al. used dual-energy CT to quantify regional density differences in the proximal humerus, identifying the posteromedial zone as the area of highest calcium concentration [16]. The present study extends these findings by providing the first depth-resolved density profile of the GT across a cohort of 739 specimens, revealing a U-shaped architecture across the full anteroposterior extent of the GT. In line with Tingart et al. [13], the posterior half of the GT profile was denser than the anterior half, and the anterior cortex reached only about 200 HU compared with 321 HU at the posterior surface.

A depth-resolved approach was previously used by Meyer et al., who sampled 5-mm cylinders in 1-mm steps from the GT surface in 14 cadaveric humeri and found a steep decline in bone volume fraction immediately beneath the cortex, with GT values of only 10–20% compared with 40% beneath the articular surface [17]. The posterior limb of the U-shaped profile in the present study reproduces this pattern in clinical CT data, and the very low or negative HU values in the GT center are consistent with the "hollow" tuberosity described in their specimens. Whereas Meyer et al. sampled from the footprint surface inward, the present ROI traversed the GT anteroposteriorly and thereby captured both cortical boundaries. Regional findings differ in part: Meyer et al. found more cancellous bone in the anterior than in the posterior GT, whereas Tingart et al. reported higher trabecular density posteriorly [11, 13] and the present data showed higher density in the posterior half of the profile; these differences may be

explained by differences in sampling direction, depth, and imaging modality. Additionally, Meyer et al. reported that the cortical shell was preserved in the presence of rotator cuff tears [17]. The largest absolute age-related decline of the cortical shell in the present study therefore suggests that age and tear-related disuse may affect the GT compartments differently, although HU values at clinical CT resolution reflect both cortical mineralization and cortical thickness.

The most directly comparable prior study is the high-resolution peripheral quantitative CT (HR-pQCT) cadaveric analysis by Kirchhoff et al., who were able to show in 64 specimens that age and sex are determinants of trabecular bone quality within the rotator cuff footprint [24]. Our findings extend their observations to an 11.5-fold larger cohort of clinical CT scans and add depth-resolved spatial information. The GT showed a decline of 12.7 HU per decade, which is consistent with the general pattern of age-related trabecular bone loss in the proximal humerus [13, 24], but slower than the decline at the calcar in the same specimens (− 22.2 HU per decade). The cross-sectional sex difference in GT density was largest in the 41–65 age group and did not widen further thereafter; given the non-significant age × sex interaction, this pattern should be interpreted with caution. Interestingly, the age–density relationship was not strictly linear: both quadratic and two-segment models indicated a deceleration of density loss in older age (breakpoint 60 years in the whole cohort and 55–60 years in women), which may partly reflect a floor effect rather than true biological stabilization, as well as survivor and cohort effects inherent to the cross-sectional design — at very low HU values, there is little remaining mineral to lose. The breakpoints should be regarded as approximate, as the fit was nearly identical across neighboring candidates.

GT and Calcar: Correlated Sites with Different Density Levels

On average, the GT was less dense than the calcar in all subgroups (overall paired d = − 0.80), and GT and calcar density were strongly correlated within specimens (r = 0.716; 0.587 after adjustment for age and sex), suggesting that proximal humeral bone density is in part determined by systemic factors. At a common threshold of 100 HU, low calcar density was almost always accompanied by low GT density (91%), whereas only 59% of specimens with low GT density also had low calcar density. This asymmetry, however, follows arithmetically from the different prevalence of values below 100 HU at the two sites (63% at the GT vs. 41% at the calcar); the ratio of the two conditional probabilities equals the ratio of these prevalences. Furthermore, the GT–calcar difference narrowed rather than widened with age, because the calcar lost density faster. The data therefore do not indicate a selective vulnerability of the GT; rather, the GT is, on average, the lower-density site throughout adult life. At the individual level, however, GT density exceeded calcar density in about one in five specimens and in more than one third of older women, so neither site can substitute for the other in the individual patient.

The clinically relevant consequence is that absolute density thresholds are site-specific. A surgeon who identifies poor calcar bone quality — whether on preoperative CT or intraoperatively — can reasonably expect that the GT is also compromised in most cases. Conversely, a calcar density that appears

adequate does not exclude low GT density, and a threshold derived from calcar data would underestimate the proportion of patients with low GT density. Fixation strategies validated in calcar bone, or bone density assessments based on calcar measurements, should therefore not be transferred to the GT without site-specific assessment.

Functional Cortical Thickness as a Bone Quality Metric

The FCT metric introduced here quantifies the depth of bone at or above a given density threshold from the cortical surface inward. Unlike mean density, which averages over the entire cross-section, FCT captures the thickness of the functional cortical shell — the zone that is most relevant to any implant relying on cortical or near-cortical fixation. As a CT-derived functional metric, FCT does not equate to histomorphometric cortical thickness but rather approximates the depth of structurally meaningful bone from the surface inward. Because the GT cylinder spanned the individual anteroposterior dimension of the GT, the sampling increment differed between specimens and was smaller in women than in men; FCT was therefore expressed in increments, with a specimen-specific millimeter equivalent. Expressed in millimeters, the FCT difference between young men and young women (4.0 vs. 2.9 mm) was larger than in increments, as the female GT was also smaller. FCT-200 and mean GT density were correlated but not interchangeable ($r = 0.770$; $R^2 = 0.593$), indicating that FCT captures information not fully reflected in mean density — possibly because mean density is also strongly influenced by the low-density cancellous center. In 69% of women older than 65 years, FCT-200 did not exceed one increment, and the logistic regression showed a 50% probability of this finding by age 56, indicating that reduced functional cortical thickness is already common in women in their late fifties. Whether this metric has utility beyond the GT as a standardized approach to quantifying regional cortical quality from CT data warrants further investigation.

Implications for Implant Fixation

Although the measurement cylinder traverses the GT along its anteroposterior axis rather than along a suture anchor insertion path, the density profile characterizes the cross-sectional bone architecture that any implant placed in the GT must contend with. Two findings are particularly relevant.

First, the cortical shell of the GT — the primary fixation substrate for all-suture anchors, which achieve fixation through subcortical deployment [7] — showed the largest absolute decline of any GT zone (− 22.7 HU per decade). Ntalos et al. reported that the pullout strength of all-suture anchors correlated strongly with the adjacent cortical thickness ($r = 0.82$), with at least 0.4 mm required to withstand 200 N [7]. In women older than 65, mean cortical shell density fell below 200 HU (180.1 HU; Table 4), and in 69% the functional cortex at 200 HU did not extend beyond the first sampling increment (in about one third of these, not even the surface point reached 200 HU). At the resolution of the present profile (approximately 1.15 mm in older women), it cannot be determined whether this residual cortex falls below the 0.4 mm reported by Ntalos et al.; the findings nevertheless identify a population in which the cortical substrate is markedly reduced. Comparable findings have been reported for screw-type anchors: Tingart et al. found

that the pull-out strength of metal screw-type anchors correlated with cortical (r = 0.63), but not with trabecular, volumetric bone mineral density of the GT, and that pull-out strength in the proximal GT was lowest posteriorly despite the highest trabecular density in this region [11]. In line with these data, the age-related decline of the cortical shell observed here suggests that near-surface bone may be relevant for anchor fixation irrespective of anchor design, and that mean or trabecular density alone may not adequately reflect fixation capacity. This provides a rationale for surface-oriented metrics such as FCT, which, however, remain to be validated biomechanically. The logistic regression analysis showed that the probability of FCT-200 ≤ 1 increment exceeded 50% by age 56 in women, i.e., in the age range of the perimenopausal transition; because menopausal status was not available in this dataset, this association remains hypothetical.

Second, beyond the cortical shell, the deep cancellous center had a mean density of only 16.2 HU overall (− 10.4 HU in older women). This is consistent with the very low trabecular bone volume fraction reported by Kirchhoff et al. within the rotator cuff footprint compared with the subarticular bone [24]. Meyer et al. similarly described a low cancellous bone volume fraction in the GT and recommended placing anchors subcortically or medially beneath the articular surface, where cancellous bone stock is higher, and avoiding a deep cancellous trough [17]. Tingart et al. reported higher trabecular bone mineral density and higher anchor failure loads in the proximal than in the distal GT [11]. Because the ROI in the present study was located on average 11 mm below the superior GT cortex, the density values reported here may underestimate bone quality at more proximal or medial insertion sites. Mean GT density below 50 HU — observed in 60% of women older than 65 — indicates very poor cancellous bone stock, in which fixation relying on cancellous purchase is likely to be compromised; this assumption has not been validated biomechanically. These patients may benefit from alternative strategies such as transosseous repair [25], cement augmentation [26–28], or bridging constructs that distribute load beyond the GT [29].

Clinical Implications

These population-level data suggest a potential role for preoperative bone quality assessment in patients undergoing rotator cuff repair. While CT-based opportunistic screening for osteoporosis is increasingly used in other contexts [21, 22], including shoulder CT [30], the standard preoperative imaging for rotator cuff pathology is magnetic resonance imaging (MRI), not CT. However, simple radiographic parameters such as proximal humeral cortical bone thickness on standard anteroposterior radiographs have recently been shown to independently predict intraoperative anchor instability — notably, without correlation to lumbar or femoral DXA values [31] — offering a practical screening tool that does not require additional imaging and underscoring the need for site-specific bone quality assessment. For patients who do undergo CT — as in fracture management or arthroplasty planning — the threshold data presented here could inform bone quality assessment: a mean GT density below 50 HU (observed in 60% of women > 65) or an FCT-200 of at most one increment (observed in 69% of women > 65) could flag patients at elevated risk for fixation failure. Prospective clinical validation of such thresholds would be required before implementation.

Furthermore, the GT density data are relevant to fracture fixation beyond rotator cuff repair. The GT is a key component of proximal humerus fracture patterns (Neer classification), and anatomic reduction with stable GT fixation is a critical determinant of functional outcome [4]. Plate and screw constructs that rely on GT bone stock for screw purchase face the same density challenges identified here, and recent evidence confirms that low CT-measured bone density — whether assessed in the humeral head [32] or the glenoid vault [33] — is associated with fixation failure. CT-derived bone density of the proximal humerus correlates strongly with systemic DXA-measured bone mineral density [34], supporting the use of opportunistic HU assessment as a practical screening tool. In the context of reverse shoulder arthroplasty with GT osteotomy, knowledge of regional bone quality may inform decisions regarding tuberosity reattachment technique.

Limitations

This study has several limitations. One limitation is that HU values were used as a proxy for bone mineral density without external phantom calibration. Although standardized 3D registration reduces inter-scanner variability, absolute density values cannot be directly compared with DXA- or quantitative CT-based measurements, and tube voltage differences across scanners may introduce systematic HU variation [35]. Furthermore, rotator cuff integrity was not known for the CT scans included in the database. Because full-thickness rotator cuff tears are associated with a marked loss of cancellous bone in the GT and humeral head [17], and their prevalence increases with age [1–3], part of the age-related decline observed here may reflect tear-related disuse rather than aging alone. Another limitation is the spatial resolution of the density profile: because the GT cylinder spanned the individual anteroposterior dimension of the GT, the sampling increment was specimen-specific (mean 1.28 mm; smaller in women than in men), and depth is expressed in relative terms. Depth zones in millimeters are therefore approximations based on mean cylinder length, and FCT is a functional approximation based on density thresholds at this resolution, not a histomorphometric measurement of cortical thickness. Furthermore, the clinical implications regarding anchor fixation are derived from density data alone, without biomechanical pullout testing. While our findings are consistent with published biomechanical data, the relationship between HU values and fixation failure thresholds has not been formally validated. A limiting factor is that all specimens were left humeri from a predominantly White cohort (80%), limiting generalizability to other populations or to potential left-right asymmetry, although Kirchhoff et al. found no significant side difference in GT bone quality parameters [24]. Asian ethnicity was associated with lower GT density independent of age and sex, but the subgroup was too small for stratified reference values, and confounding by institution or scanner cannot be excluded. Another limiting factor is that the GT and calcar ROIs differed in geometry (bicortical GT cylinder of specimen-specific length vs. calcar cylinder of fixed length), so that absolute between-site differences may partly reflect differences in the proportion of cortical bone sampled. Unfortunately, body mass index (BMI) data were available for only 347 of 739 specimens (47%), and this subsample was considerably older than the remaining cohort (70.2 vs. 49.4 years), precluding meaningful analysis of the BMI-density relationship. Additionally, although Bonferroni correction was applied for pairwise age-group comparisons, the overall number of

statistical tests across subgroups, depth points, and threshold analyses was large, which increases the risk of type I error; the majority of reported p-values were well below 0.001, mitigating this concern, but the exploratory subgroup analyses should be considered hypothesis-generating. The mean HU distributions deviated significantly from normality in several subgroups; given the large subgroup sizes, the parametric analyses are considered robust. The 21 measurement points along the cylinder axis are spatially correlated, and the depth-specific regression analyses do not account for this correlation structure; a mixed-effects model treating depth as a repeated measure would be a more formal approach to testing depth-dependent effects. Finally, the breakpoints of the two-segment models were selected as the R^2-maximizing value among seven candidates, so the associated F-tests are not adjusted for this selection, and the non-linear models provided only modest improvement over the linear fit (R^2 increase of 0.026). As the data are cross-sectional, age-related differences cannot be interpreted as individual longitudinal bone loss.

Conclusions

The GT exhibits a U-shaped bone density architecture with a thin functional cortical shell that shows the largest absolute decline with aging. In most women older than 65 years, the functional cortex at 200 HU did not exceed one sampling increment, and this finding was already common from the late fifties; the cancellous center had negative mean HU values in older women. Because the GT is, on average, the lower-density site compared with the calcar in all age and sex subgroups, calcar-derived density thresholds should not be assumed to apply to the GT, and site-specific assessment is recommended when GT fixation quality is critical.

Abbreviations

ANCOVA
Analysis of covariance
BMI
Body mass index
CI
Confidence interval
CT
Computed tomography
DXA
Dual-energy X-ray absorptiometry
FCT
Functional cortical thickness
GT
Greater tuberosity
HR-pQCT
High-resolution peripheral quantitative computed tomography

HU
Hounsfield units
MRI
Magnetic resonance imaging
pQCT
Peripheral quantitative computed tomography
ROI
Region of interest
SD
Standard deviation
SOMA
Stryker Orthopaedic Modeling and Analytics
STROBE
Strengthening the Reporting of Observational Studies in Epidemiology

Declarations

Ethics approval and consent to participate

This study was conducted in accordance with the Declaration of Helsinki. The Ethics Committee of the Hamburg Medical Association (Ethikkommission der Ärztekammer Hamburg; reference number 2023-300394-WF) confirmed that formal ethical approval was not required for this study, as it exclusively used fully anonymized imaging data. Informed consent was not applicable, as all data were fully anonymized before access.

Consent for publication

Not applicable.

Clinical trial number

Not applicable.

Availability of data and materials

The datasets analyzed during the current study are not publicly available due to proprietary restrictions of the SOMA database but are available from the corresponding author on reasonable request and with permission from Stryker Trauma GmbH.

Competing interests

LEJG was employed by Stryker Trauma GmbH during the conduct of this study. BH is a current employee of Stryker Trauma GmbH. The remaining authors declare that they have no competing interests.

Funding

This research received no specific grant from any funding agency in the public, commercial, or not-for-profit sectors. Stryker Trauma GmbH provided access to the SOMA database for research purposes; no financial support was received.

Authors' contributions

MFF contributed to conceptualization, methodology, and writing (original draft). FS and SIS contributed to investigation and data curation. LEJG and BH contributed to data acquisition, technical support, and critical revision of the manuscript. HK contributed to methodology. DT contributed to methodology and critical revision of the manuscript. KHF contributed to conceptualization and supervision. LFH contributed to conceptualization, methodology, formal analysis, data curation, and writing (original draft). All authors critically revised the manuscript and approved the final version.

Acknowledgements

The authors acknowledge Stryker Trauma GmbH for providing access to the SOMA database for research purposes.

References

1. Minagawa H, Yamamoto N, Abe H, Fukuda M, Seki N, Kikuchi K, et al. Prevalence of symptomatic and asymptomatic rotator cuff tears in the general population: From mass-screening in one village. J Orthop. 2013;10:8–12. https://doi.org/10.1016/j.jor.2013.01.008.
2. Tashjian RZ. Epidemiology, natural history, and indications for treatment of rotator cuff tears. Clin Sports Med. 2012;31:589–604. https://doi.org/10.1016/j.csm.2012.07.001.
3. Yamamoto A, Takagishi K, Osawa T, Yanagawa T, Nakajima D, Shitara H, et al. Prevalence and risk factors of a rotator cuff tear in the general population. J Shoulder Elb Surg. 2010;19:116–20. https://doi.org/10.1016/j.jse.2009.04.006.
4. Rudran B, Little C, Duff A, Poon H, Tang Q. Proximal humerus fractures: anatomy, diagnosis and management. Br J Hosp Med. 2022;83(7):1–10. https://doi.org/10.12968/hmed.2021.0554.
5. Barber FA, Feder SM, Burkhart SS, Ahrens J. The relationship of suture anchor failure and bone density to proximal humerus location: a cadaveric study. Arthroscopy. 1997;13:340–5. https://doi.org/10.1016/s0749-8063(97)90031-1.
6. Poukalova M, Yakacki CM, Guldberg RE, Lin A, Saing M, Gillogly SD, et al. Pullout strength of suture anchors: effect of mechanical properties of trabecular bone. J Biomech. 2010;43:1138–45. https://doi.org/10.1016/j.jbiomech.2009.12.007.
7. Ntalos D, Huber G, Sellenschloh K, Saito H, Püschel K, Morlock MM, et al. All-suture anchor pullout results in decreased bone damage and depends on cortical thickness. Knee Surg Sports Traumatol Arthrosc. 2021;29:2212–9. https://doi.org/10.1007/s00167-020-06004-6.

8. Braunstein V, Ockert B, Windolf M, Sprecher CM, Mutschler W, Imhoff A, et al. Increasing pullout strength of suture anchors in osteoporotic bone using augmentation — a cadaver study. Clin Biomech (Bristol Avon). 2015;30(3):243–7. https://doi.org/10.1016/j.clinbiomech.2015.02.002.
9. Ntalos D, Huber G, Sellenschloh K, Briem D, Püschel K, Morlock MM, et al. Biomechanical analysis of conventional anchor revision after all-suture anchor pullout: a human cadaveric shoulder model. J Shoulder Elb Surg. 2019;28:2433–7. https://doi.org/10.1016/j.jse.2019.04.053.
10. Pietschmann MF, Hölzer A, Rösl C, Scharpf A, Niethammer T, Jansson V, et al. What humeri are suitable for comparative testing of suture anchors? An ultrastructural bone analysis and biomechanical study of ovine, bovine and human humeri and four different anchor types. J Biomech. 2010;43:1125–30. https://doi.org/10.1016/j.jbiomech.2009.12.021.
11. Tingart MJ, Apreleva M, Lehtinen J, Zurakowski D, Warner JJP. Anchor design and bone mineral density affect the pull-out strength of suture anchors in rotator cuff repair: which anchors are best to use in patients with low bone quality? Am J Sports Med. 2004;32:1466–73. https://doi.org/10.1177/0363546503262644.
12. Hyatt AE, Lavery K, Mino C, Dhawan A. Suture anchor biomechanics after rotator cuff footprint decortication. Arthroscopy. 2016;32. https://doi.org/10.1016/j.arthro.2015.08.034. :544 – 50.
13. Tingart MJ, Bouxsein ML, Zurakowski D, Warner JP, Apreleva M. Three-dimensional distribution of bone density in the proximal humerus. Calcif Tissue Int. 2003;73:531–6. https://doi.org/10.1007/s00223-002-0013-9.
14. Tingart MJ, Lehtinen J, Zurakowski D, Warner JJP, Apreleva M. Proximal humeral fractures: regional differences in bone mineral density of the humeral head affect the fixation strength of cancellous screws. J Shoulder Elb Surg. 2006;15:620–4. https://doi.org/10.1016/j.jse.2005.09.007.
15. Spross C, Kaestle N, Benninger E, Fornaro J, Erhardt J, Zdravkovic V, et al. Deltoid Tuberosity Index: a simple radiographic tool to assess local bone quality in proximal humerus fractures. Clin Orthop Relat Res. 2015;473:3038–45. https://doi.org/10.1007/s11999-015-4322-x.
16. Yu Q, Yang J, Zhou C, Xu Z, Liu C, Luo Q, et al. Quantification of bone quality and distribution of the proximal humerus with dual-energy computed tomography. Quant Imaging Med Surg. 2023;13:5676–87. https://doi.org/10.21037/qims-22-927.
17. Meyer DC, Fucentese SF, Koller B, Gerber C. Association of osteopenia of the humeral head with full-thickness rotator cuff tears. J Shoulder Elb Surg. 2004;13:333–7. https://doi.org/10.1016/j.jse.2003.12.016.
18. Kleinertz H, Mueller E, Leonhardt LG, Thiesen DM, Hofstätter B, Petersik A, et al. Bone mass distribution of 892 distal tibiae and implications for the treatment of medial malleolar fractures. Foot Ankle Surg. 2025;31:436–42. https://doi.org/10.1016/j.fas.2025.01.007.
19. Thiesen DM, Ntalos D, Berger-Groch J, Petersik A, Hofstätter B, Frosch KH, et al. The three-dimensional bone mass distribution of the posterior pelvic ring and its key role in transsacral screw placement. Sci Rep. 2020;10:5690. https://doi.org/10.1038/s41598-020-61954-8.

20. Schröder M, Gottschling H, Reimers N, Hauschild M, Burgkart R. Automated morphometric analysis of the femur on large anatomical databases with highly accurate correspondence detection. Open Med J. 2014;1:15–22. https://doi.org/10.2174/1874220301401010015.
21. Hendrickson NR, Pickhardt PJ, Del Rio AM, Rosas HG, Anderson PA. Bone mineral density T-scores derived from CT attenuation numbers (Hounsfield units): clinical utility and correlation with dual-energy X-ray absorptiometry. Iowa Orthop J. 2018;38:25–31.
22. Schreiber JJ, Anderson PA, Rosas HG, Buchholz AL, Au AG. Hounsfield units for assessing bone mineral density and strength: a tool for osteoporosis management. J Bone Joint Surg Am. 2011;93:1057–63. https://doi.org/10.2106/JBJS.J.00160.
23. Pervaiz K, Cabezas A, Downes K, Santoni BG, Frankle MA. Osteoporosis and shoulder osteoarthritis: incidence, risk factors, and surgical implications. J Shoulder Elb Surg. 2013;22:e1–8. https://doi.org/10.1016/j.jse.2012.05.029.
24. Kirchhoff C, Braunstein V, Milz S, Sprecher CM, Kirchhoff S, Graw M, et al. Age and gender as determinants of the bone quality of the greater tuberosity: a HR-pQCT cadaver study. BMC Musculoskelet Disord. 2012;13:221. https://doi.org/10.1186/1471-2474-13-221.
25. Sandow MJ, Schutz CR. Arthroscopic rotator cuff repair using a transosseous knotless anchor (ATOK). J Shoulder Elb Surg. 2020;29:527–33. https://doi.org/10.1016/j.jse.2019.07.017.
26. Diaz MA, Branch EA, Paredes LA, Oakley E, Baker CE. Calcium phosphate bone void filler increases threaded suture anchor pullout strength: a biomechanical study. Arthroscopy. 2020;36:1000–8. https://doi.org/10.1016/j.arthro.2019.12.003.
27. Diaz MA, Munassi S, Teytelbaum DE, Pipitone A, Baker CE. An injectable calcium phosphate bone graft substitute improves the pullout strength of various suture anchor designs in an osteoporotic bone model. Arthrosc Sports Med Rehabil. 2023;5:e423–33. https://doi.org/10.1016/j.asmr.2023.01.010.
28. Heilig P, Jordan MC, Paul MM, Kupczyk E, Meffert RH, Gbureck U, et al. Augmentation of suture anchors with magnesium phosphate cement — simple technique with striking effect. J Mech Behav Biomed Mater. 2022;128:105096. https://doi.org/10.1016/j.jmbbm.2022.105096.
29. Entezari V, Lazarus M. Surgical considerations in managing osteoporosis, osteopenia, and vitamin D deficiency during arthroscopic rotator cuff repair. Orthop Clin North Am. 2019;50:233–43. https://doi.org/10.1016/j.ocl.2018.10.006.
30. Sebro R, De la Garza-Ramos C. Can we screen opportunistically for low bone mineral density using CT scans of the shoulder and artificial intelligence? Br J Radiol. 2024;97:1450–60. https://doi.org/10.1093/bjr/tqae109.
31. Igrek S, Yigit O, Erem M, Canbaz SB, Eceviz E, Kocaoglu B. Measurement of proximal humeral cortical bone thickness to predict intraoperative anchor stability in arthroscopic rotator cuff repair. Orthop J Sports Med. 2026;14:23259671261427779. https://doi.org/10.1177/23259671261427779.
32. Varga P, Grünwald L, Windolf M. The prediction of cyclic proximal humerus fracture fixation failure by various bone density measures. J Orthop Res. 2018;36:2250–8.

https://doi.org/10.1002/jor.23879.
33. Czerwonka N, Mastroianni MA, Hellwinkel JE, Malka M, Kirkwood G, Arvind V, et al. Low glenoid vault bone density is a risk factor for failure of proximal humerus fracture fixation. J Shoulder Elb Surg. 2026;35:1185–93. https://doi.org/10.1016/j.jse.2025.09.008.
34. Zhang X, Zhu CX, He JQ, Hu YC, Sun J. Correlation of CT values and bone mineral density in elderly Chinese patients with proximal humeral fractures. Orthop Surg. 2021;13:2271–9. https://doi.org/10.1111/os.13145.
35. Garner HW, Paturzo MM, Gaudier G, Pickhardt PJ, Wessell DE. Variation in attenuation in L1 trabecular bone at different tube voltages: caution is warranted when screening for osteoporosis with the use of opportunistic CT. AJR Am J Roentgenol. 2017;208:165–70. https://doi.org/10.2214/AJR.16.16744.

Figures

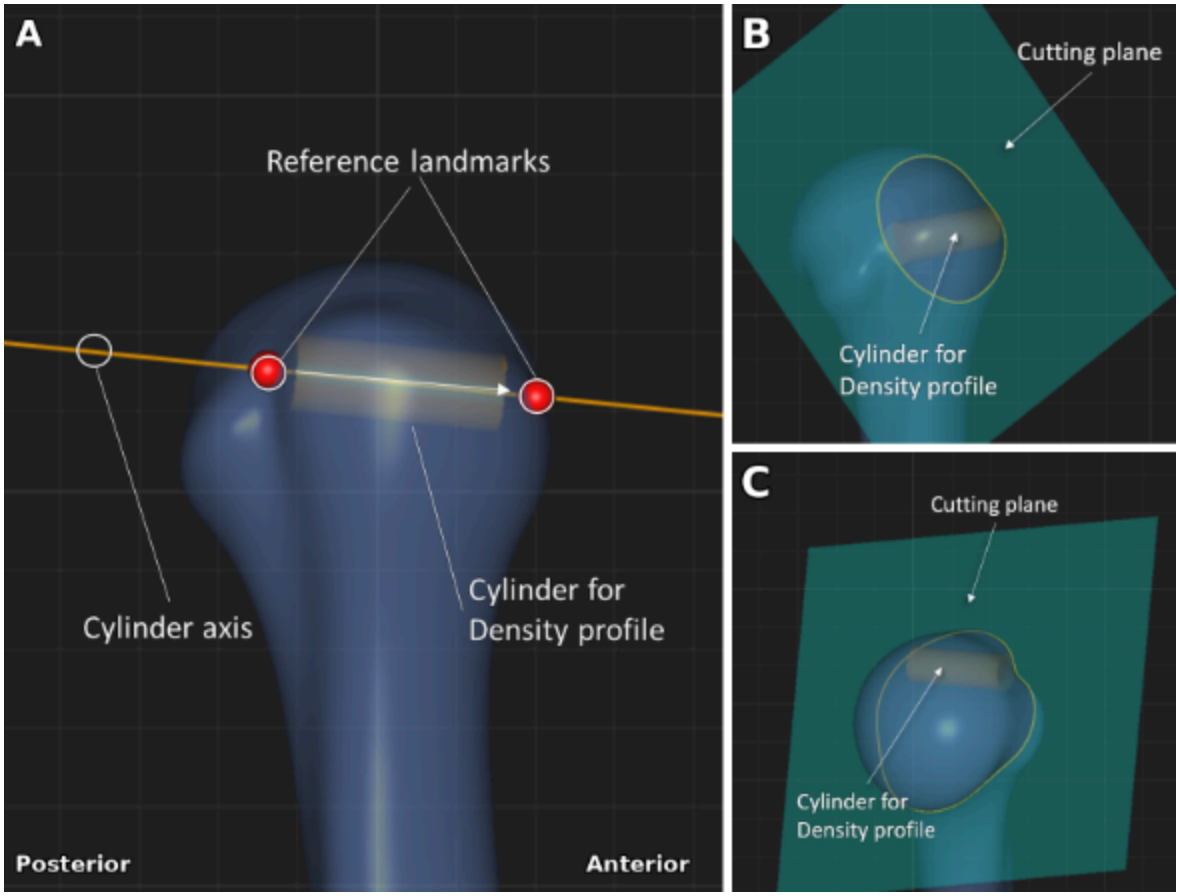


Figure 1

Placement of the greater tuberosity (GT) region of interest. Three-dimensional model of the proximal humerus with the cylindrical region of interest (5 mm diameter) along the anteroposterior axis, spanning from the posterior to the anterior cortex. All panels show the GT region of interest. **(A)** Cylinder axis (posterior → anterior) and the two reference landmarks (red dots) defining the cylinder. **(B)** Oblique

cutting plane containing the cylinder axis through the GT. **(C)** Cutting plane through the humeral head at the level of the GT cylinder, used for the density heatmaps in Fig. 3.

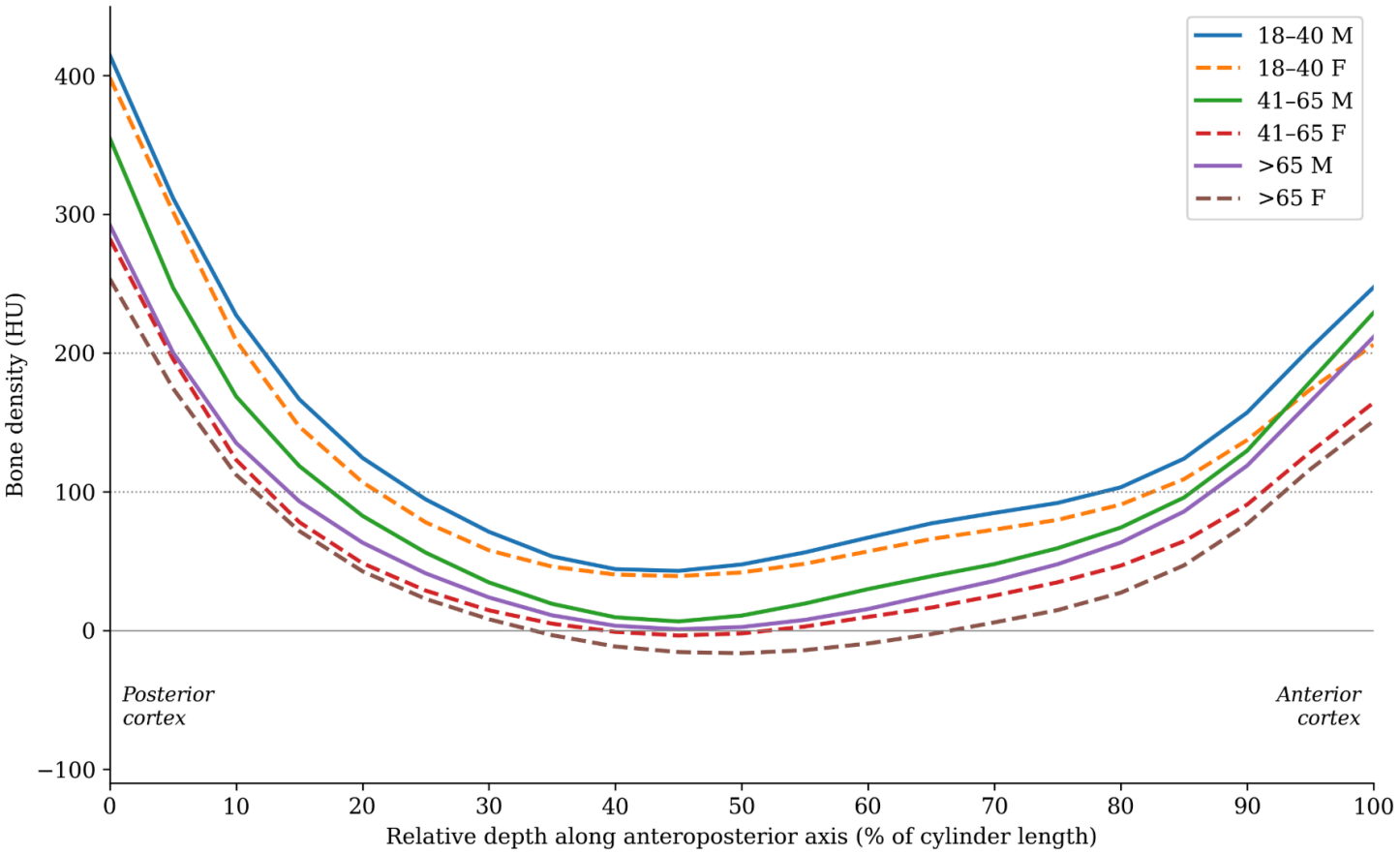


Figure 2

Bone density profile of the greater tuberosity by age and sex subgroup. Density (HU) along the anteroposterior axis is plotted against relative depth (0% = posterior cortex, 100% = anterior cortex; one 5% increment corresponds to 1.28 ± 0.16 mm on average). Note the characteristic U-shape reflecting the cortex–cancellous–cortex architecture, with a minimum at 45–50% depth. Horizontal lines indicate 200 HU and 100 HU thresholds.

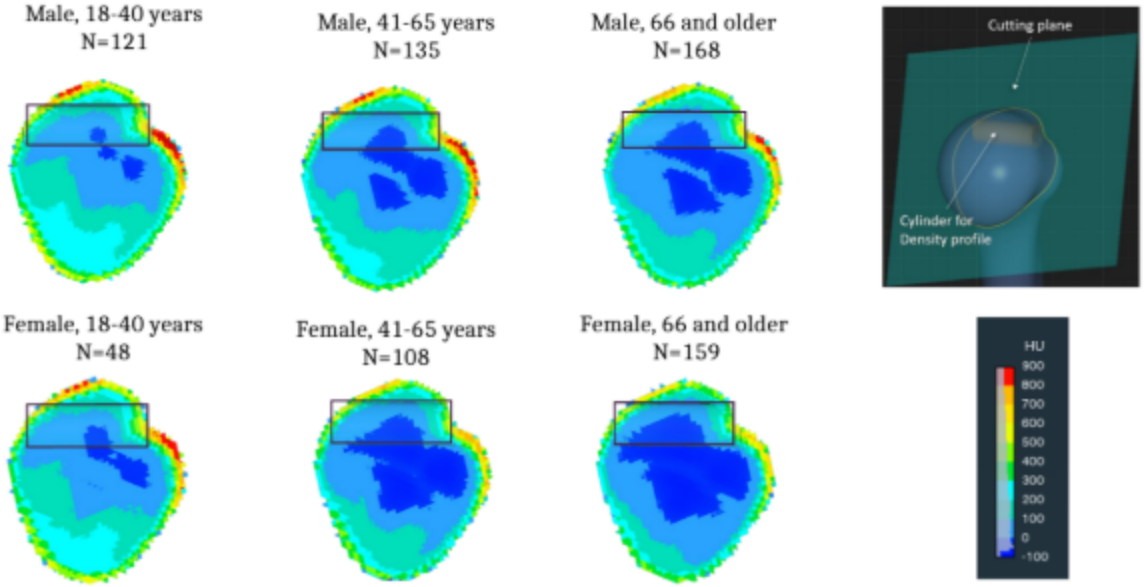


Figure 3

Bone density heatmaps at the level of the greater tuberosity cylinder by age and sex. Heatmaps are shown on the cutting plane through the humeral head (inset; see Fig. 1C). Each panel represents the mean Hounsfield unit value of the averaged bone model for a given subgroup. The rectangle indicates the cylindrical region of interest from which the density profile was extracted. The color scale ranges from −100 HU (blue) to 900 HU (red). Note the expansion of the low-density central zone with increasing age, most pronounced in women older than 65 years.

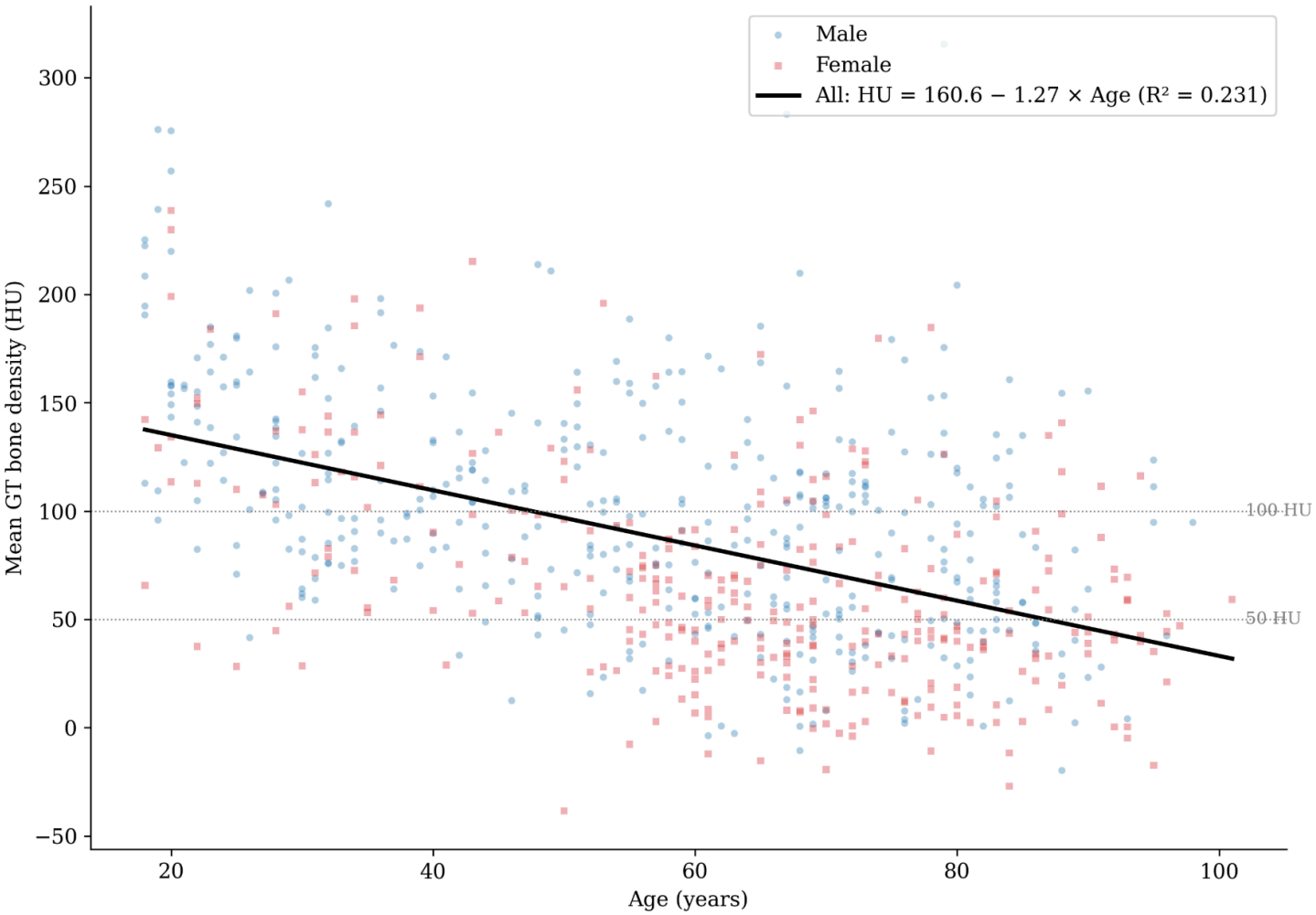


Figure 4

Regression of mean greater tuberosity density (HU) on age. Each data point represents the mean density across all 21 measurement points for one specimen. The regression line represents the overall linear model (HU = 160.6 − 1.27 × Age; R^2 = 0.231). Horizontal reference lines indicate the 100 HU and 50 HU thresholds.

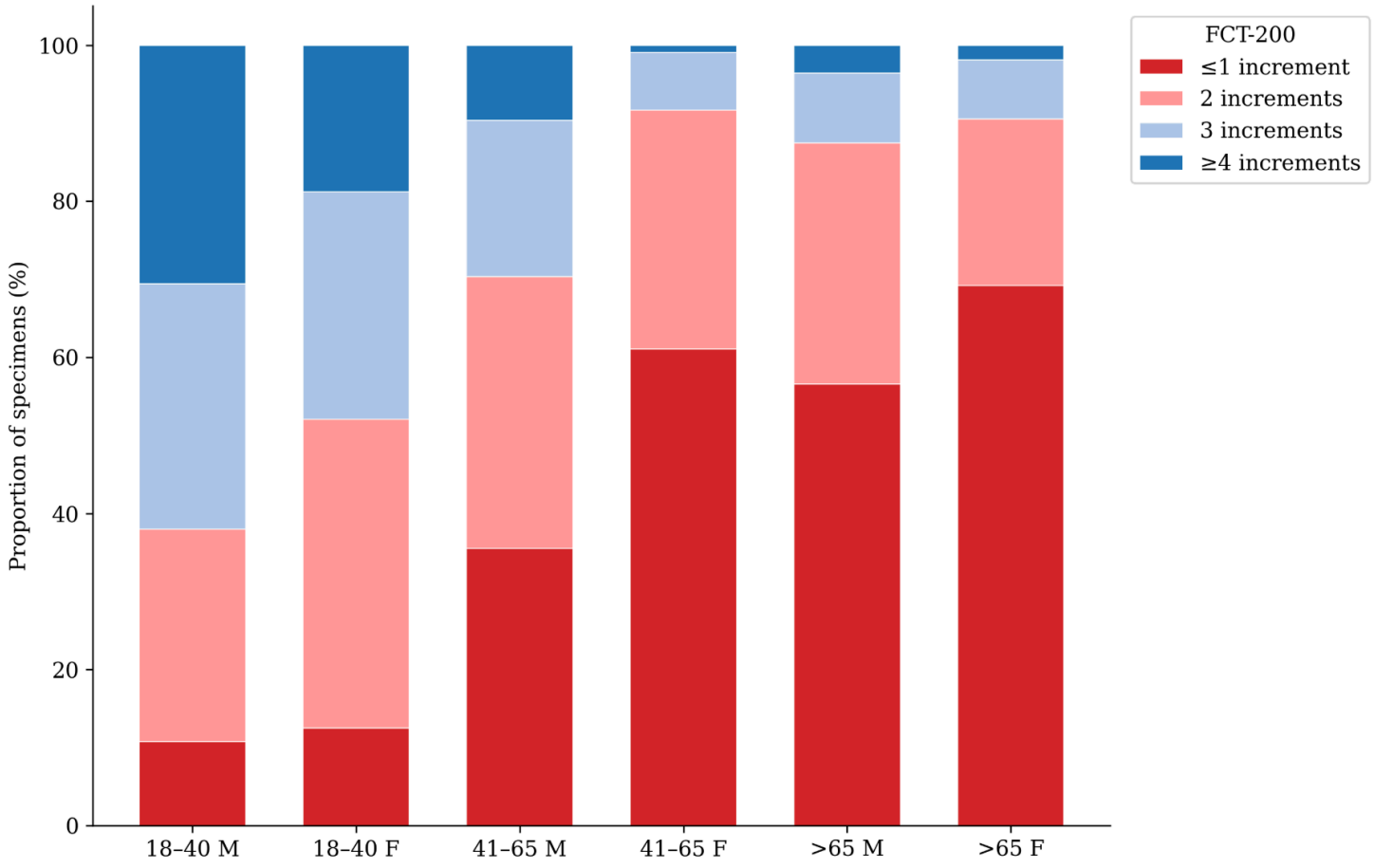


Figure 5

Functional cortical thickness at 200 HU (FCT-200) by age and sex subgroup. Stacked bars show the proportion of specimens in each FCT-200 category (≤1, 2, 3, and ≥4 sampling increments). Note the progressive shift toward thinner functional cortex with increasing age, with 69.2% of women older than 65 years having FCT-200 ≤1 increment.

Supplementary Files

This is a list of supplementary files associated with this preprint. Click to download.

- Additionalfile2Depthprofiletable.docx
- Additionalfile1STROBEchecklist.docx